Transparency in two-level spin systems induced by a longitudinal field

Moritz Kälin, Igor Gromov,* and Arthur Schweiger†
Physical Chemistry, ETH Zürich, CH-8093 Zürich, Switzerland
(Received 19 May 2003; published 17 March 2004)

In an electron-spin two-level system a bichromatic radiation field, consisting of a transverse microwave field and a radio frequency field oriented parallel to the static magnetic field, can induce multiple photon transitions of the type $\sigma^+_{\mathrm{mw}}+k\pi_{\mathrm{rf}}$, with the photons σ^+_{mw} and π_{rf} absorbed from the microwave and radio frequency fields, and k being an integer. The two-level spin system may become transparent under such a bichromatic radiation field. This phenomenon directly depends on the presence of the π photons of the longitudinal radio frequency field. An analytical description of the multiple photon processes and the resulting transparency effects, based on a toggling-frame approach, is given. The effective field amplitudes of the multiple photon transitions are found to have a Bessel-function-like dependence on the radio frequency amplitude. The behavior of the magnetization vector during a bichromatic pulse is illustrated by using classical equations of motion. The theoretically predicted effects are verified experimentally. As an example for an application of the investigated type of electromagnetically induced transparency, a one-pulse echo experiment is described, where the free evolution period is created artificially.

DOI: 10.1103/PhysRevA.69.033809 PACS number(s): 42.50.Gy, 33.35.+r, 32.80.Wr

I. INTRODUCTION

There are different means to make an opaque medium transparent. In the case of *self-induced transparency* the material becomes transparent when the flip angle of a radiation pulse applied to a two-level system reaches 2π. In this experiment, first described in optics by McCall and Hahn in 1969 [1], a light pulse propagates through many Beer's absorption lengths of a dense medium. Self-induced transparency has also been observed in electron paramagnetic resonance (EPR), using so-called zero-area pulse propagation, where the phase of the microwave (mw) radiation is changed during the pulse [2].

More recently, *electromagnetically induced transparency* (EIT) has been described [3–6]. In EIT a coherent superposition of two states is prepared by irradiating the system with a resonant pump laser. The electric dipole moments of the two transitions that connect these two levels with a third level show then destructive interference [3]. As a result a resonant probe laser can no longer induce transitions; the system is transparent. EIT has also been observed in electron–nuclear-spin systems with pulse EPR [7], and with optically detected continuous-wave (cw) EPR [8,9].

It was shown that EIT can also take place in two-level systems [10]. An atomic two-level system in a strong-coupling field can become transparent to a second probe field due to quantum interference between different multiple photon transition pathways. The behavior of two-level atoms subject to a bichromatic field nearly resonant to the transition was studied using different approaches [11–17]. Consistently, a fluorescence spectrum is predicted that shows lines at various subharmonics of the used laser frequencies, which fits well to the experimental results [18]. In this work we introduce a related transparency phenomenon that can be observed in two-level spin systems in a bichromatic field consisting of a mw field and a radio frequency (rf) field. The effect is also based on the destructive interference of multiple photon processes, resulting in a vanishing overall transition amplitude. The difference of our experiment to the optical experiments mentioned above lies in the fact that in our case the two fields are different in polarization and differ in the frequencies by about three orders of magnitude.

During a transition between two levels in a spin system not only the energy but also the overall angular momentum has to be conserved. In an $S=1/2$ electron-spin system with two levels, described by the magnetic spin quantum numbers $m_S=1/2$ and $m_S=-1/2$, the angular momentum is provided by photons that are absorbed from a circularly polarized radiation field, oriented perpendicular to the quantization axis of the spins (in our case the external static magnetic field $\mathbf{B}_0$). In an EPR experiment this is the right-hand circularly polarized component (σ^+ photons) of a linearly polarized mw field perpendicular to $\mathbf{B}_0$. Another possible process for which the angular momentum is conserved is the combined absorption and emission of mw σ^+ photons of different frequencies (for example, $\sigma^+_1-\sigma^+_2+\sigma^+_1$). Various cw and pulse EPR and nuclear-magnetic-resonance (NMR) experiments are based on this process [19–26].

If in an EPR experiment in addition to the mw radiation a linearly polarized strong rf field is applied *parallel* to $\mathbf{B}_0$, multiple photon transitions of the type $\sigma^+_{\mathrm{mw}}+k\pi_{\mathrm{rf}}$ are induced [27,28]. During such multiple photon transitions one mw σ^+ photon is absorbed and k rf π photons, with $m_J=0$, are absorbed or emitted. The parameter $k\in\mathbb{Z}$ describes the net number of rf π photons absorbed ($k>0$) or emitted ($k<0$) during the transition. Since π photons have zero angular momentum, there is no restriction to the number of absorbed rf photons, as long as energy conservation is fulfilled. σ^+_{mw}

*On leave from MRS Laboratory, Kazan State University, 42008 Kazan, Russian Federation.
†Electronic address: schweiger@phys.chem.ethz.ch; URL:http://www.esr.ethz.ch

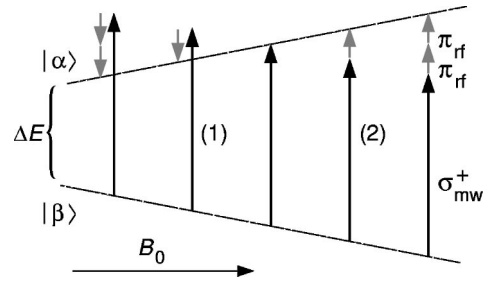

FIG. 1. Energy-level diagram of an $S=\frac{1}{2}$ spin system with multiple photon transitions of the type $\sigma^+_{\mathrm{mw}}+k\pi_{\mathrm{rf}}$, as a function of the static magnetic field B_0. (1) One mw σ^+ photon is absorbed and one rf π photon is emitted. (2) One mw σ^+ photon and one rf π photon are absorbed.

$+k\pi_{\mathrm{rf}}$ multiple photon transitions are observed at higher or lower magnetic fields (and thus called sidebands) with respect to the single-photon transition (center band), as is shown in Fig. 1. Recently we have proven that $\sigma^+_{\mathrm{mw}}+k\pi_{\mathrm{rf}}$ multiple photon transitions are the dominant features in the spectra obtained with field-modulated cw EPR spectroscopy [29,30]. They manifest as a large number of (usually unresolved) modulation sidebands and are responsible for the derivative line shape commonly observed in cw EPR spectra.

Two-photon transitions of the type $\sigma^+_{\mathrm{mw}}+\pi_{\mathrm{mw}}$ in two-level electron-spin systems have been studied extensively [31–34]. Also multiple photon transitions $\sigma^+_{\mathrm{mw}}+k\pi_{\mathrm{mw}}$ with k up to 6 have been reported [35]. The corresponding $\sigma^-_{\mathrm{rf}}+\pi_{\mathrm{rf}}$ two-photon transitions were used for excitation in NMR noise spectroscopy [36]. In cw electron–nuclear double resonance (ENDOR), lines observed at low frequencies were identified as $\sigma^+_{\mathrm{mw}}+\pi_{\mathrm{rf}}$ two-photon transitions [37].

In this study we focus on a special type of multiple photon transition, namely, the $-m\pi_{\mathrm{rf}}+\sigma^+_{\mathrm{mw}}+m\pi_{\mathrm{rf}}$ transitions, with $k\in\mathbb{Z}$. These transitions fulfill the same resonance condition as a single-photon transition. We demonstrate that for properly chosen experimental parameters of the rf field the *net transition amplitude* for the transition in a two-level spin system becomes zero. The spin system is *transparent* owing to destructive interference of the different $-m\pi_{\mathrm{rf}}+\sigma^+_{\mathrm{mw}}+m\pi_{\mathrm{rf}}$ multiple photon processes, induced by the longitudinal rf field. Corresponding effects can also be observed on the sidebands.

First, we present a theory for the description of the observed transparency, based on the toggling-frame approach introduced recently to describe multiple photon transitions in cw EPR experiments [29,30]. Then we illustrate different phenomena related to the transparency effect by using a classical vector model. The transparency phenomenon is verified experimentally by a nutation and a spin-echo experiment. Finally, we introduce a different type of echo, which can be observed after a single mw pulse by creating an artificial free evolution period during part of the pulse.

II. THEORY

A. Toggling frame

The semiclassical Hamiltonian of an $S=1/2$ electron-spin system, exposed to a linearly polarized transverse mw field along the laboratory x axis and a linearly polarized longitudinal rf field and a static magnetic field along the laboratory z axis, in angular frequency units, is given by

$$\mathcal{H}_{\mathrm{lab}}(t)=\omega_S S_z+2\omega_1\cos(\omega_{\mathrm{mw}}t+\varphi_{\mathrm{mw}})S_x+2\omega_2\cos(\omega_{\mathrm{rf}}t+\varphi_{\mathrm{rf}})S_z, \tag{1}$$

with the Larmor frequency $\omega_S=-\gamma_e B_0=g\beta_e B_0/\hbar$, the mw field with frequency ω_{mw}, phase φ_{mw}, and amplitude $2\omega_1=-\gamma_e B_{\mathrm{mw}}$, and the rf field with frequency ω_{rf}, phase φ_{rf}, and amplitude $2\omega_2=-\gamma_e B_{\mathrm{rf}}$.

If the only oscillating field is the transverse mw field, the time evolution of the spin system is usually described in the *rotating frame*, where the spin Hamiltonian is time independent [38]. In the case at hand with two radiation fields, the theoretical treatment is more involved. Recently, we introduced a *toggling-frame* transformation for the description of field-modulated cw EPR experiments in terms of $\sigma_{\mathrm{mw}}+k\pi_{\mathrm{rf}}$ multiple photon transitions [29], which will be used here for the characterization of multiple photon transitions driven by bichromatic pulses and for the description of the investigated transparency effects.

The spin Hamiltonian in Eq. (1) is transformed from the laboratory frame to the singly rotating frame

$$\begin{aligned}\mathcal{H}_{\mathrm{SRF}}(t)&=e^{i\omega_{\mathrm{mw}}tS_z}\mathcal{H}_{\mathrm{lab}}(t)e^{-i\omega_{\mathrm{mw}}tS_z}-\omega_{\mathrm{mw}}S_z\\&=[\omega_S-\omega_{\mathrm{mw}}]S_z+2\omega_2\cos(\omega_{\mathrm{rf}}t+\varphi_{\mathrm{rf}})S_z\\&\quad+\omega_1 e^{-i\varphi_{\mathrm{mw}}S_z}S_x e^{i\varphi_{\mathrm{mw}}S_z}+\omega_1 e^{i(2\omega_{\mathrm{mw}}t+\varphi_{\mathrm{mw}})S_z}\\&\quad\times S_x e^{-i(2\omega_{\mathrm{mw}}t+\varphi_{\mathrm{mw}})S_z},\end{aligned} \tag{2}$$

and then to a toggling frame

$$\mathcal{H}_{\mathrm{TF},k}(t)=R(t)\mathcal{H}_{\mathrm{SRF}}(t)R^{-1}(t)-k\omega_{\mathrm{rf}}S_z-2\omega_2\cos(\omega_{\mathrm{rf}}t+\varphi_{\mathrm{rf}})S_z, \tag{3}$$

where

$$R(t)=e^{i[k\omega_{\mathrm{rf}}t+(2\omega_2/\omega_{\mathrm{rf}})\sin(\omega_{\mathrm{rf}}t+\varphi_{\mathrm{rf}})]S_z} \tag{4}$$

is the toggling-frame rotation operator. Note that the toggling frame is not the doubly rotating frame that is regularly used to describe excitation by two transverse fields. In that case a Hamiltonian in the laboratory frame is subject to two subsequent standard rotating-frame transformations.

By neglecting the counterrotating part of the mw field, which would manifest as a Bloch-Siegert shift [39] of the energy levels, the Hamiltonian can be written as [29]

$$\begin{aligned}\mathcal{H}_{\mathrm{TF},k}(t)&=(\omega_S-\omega_{\mathrm{mw}}-k\omega_{\mathrm{rf}})S_z+\sum_{n=-\infty}^{+\infty}J_n\left(\frac{2\omega_2}{\omega_{\mathrm{rf}}}\right)\\&\quad\times\omega_1 e^{i[(k+n)\omega_{\mathrm{rf}}t+(n\varphi_{\mathrm{rf}}-\varphi_{\mathrm{mw}})]S_z}S_x e^{-i[(k+n)\omega_{\mathrm{rf}}t+(n\varphi_{\mathrm{rf}}-\varphi_{\mathrm{mw}})]S_z}.\end{aligned} \tag{5}$$

$J_n(z)$ is the Bessel function of the first kind, with order n and argument $z=2\omega_2/\omega_{\mathrm{rf}}$. In Eq. (5) only the term with $n=-k$, with amplitude $\omega_1 J_{-k}(2\omega_2/\omega_{\mathrm{rf}})$, is time independent. For weak mw fields, as commonly used in cw EPR, the time-dependent terms are small and can be neglected. For stronger mw fields, they lead to a Bloch-Siegert-like shift

$$\Delta_k = \left(\frac{2\omega_1^2}{\omega_{\rm rf}}\right)\sum_{l\neq k}\frac{J_l^2\left(\frac{2\omega_2}{\omega_{\rm rf}}\right)}{(k-l)} \tag{6}$$

of the energy levels. It can be shown that $\Delta_{-k}=-\Delta_k$. Consequently, there is no shift for the single-photon transition, $\Delta_0=0$.

The time-dependent terms also lead to higher-order corrections of the effective field amplitude. Calculated up to third order we find

$$\begin{aligned}\omega_{1,k} &= \omega_1\Bigg[J_{-k}\left(\frac{2\omega_2}{\omega_{\rm rf}}\right)+\left(\frac{\omega_1}{2\omega_{\rm rf}}\right)^2 \\ &\quad\times\sum_{l\neq k}\sum_{m\neq 0}\frac{J_{-l}\left(\frac{2\omega_2}{\omega_{\rm rf}}\right)J_{m-l}\left(\frac{2\omega_2}{\omega_{\rm rf}}\right)J_{m-k}\left(\frac{2\omega_2}{\omega_{\rm rf}}\right)}{(l-k)m}\Bigg] \\ &= \omega_1[c_k^{(1)}+c_k^{(3)}].\end{aligned} \tag{7}$$

The first-order coefficient $c_k^{(1)}$ in Eq. (7) describes the effective field $\omega_{1,k}$ for $\omega_1 \ll \omega_{\rm rf}$. For larger values of ω_1 the third-order term $c_k^{(3)}$ becomes relevant. Note that the original expression for $c_k^{(3)}$ in Ref. [29] contains a sign error. The effective spin Hamiltonian in the toggling frame may then be written as

$$\mathcal{H}_{{\rm TF},k} = ([\omega_S+\Delta_k]-[\omega_{\rm mw}+k\omega_{\rm rf}])S_z + \omega_{1,k}e^{-i\varphi_k S_z}S_x e^{i\varphi_k S_z}, \tag{8}$$

where $\varphi_k=\varphi_{\rm mw}+k\varphi_{\rm rf}$ is the phase of the effective field. The Hamiltonian in Eq. (8) essentially describes the spin system exposed to an effective radiation field with frequency $\omega_{\rm mw}+k\omega_{\rm rf}$, phase φ_k, and amplitude $\omega_{1,k}$.

Note that the Hamiltonian in Eq. (8) is based on the assumption that the quantization axis in the singly rotating frame is oriented approximately along the z axis. The mw field is treated as a weak perturbation of the diagonal part of the Hamiltonian in Eq. (3). This approach is valid as long as the mw field ω_1 is smaller than the resonance offset $\Omega_S=\omega_S-\omega_{\rm mw}$, which is normally the case for multiple photon transitions with $|k|>1$. For the single-photon transition, on the other hand, ω_1 may easily exceed Ω_S. Thus for larger mw amplitudes the quantization axis in the singly rotating frame has to be oriented along the effective field vector $\boldsymbol{\omega}_{\rm eff}=\boldsymbol{\Omega}_S+\boldsymbol{\omega}_1$. This is achieved by a rotation about the y axis by the angle $\theta=\arctan(\omega_1/\Omega_S)$. With the mw phase $\varphi_{\rm mw}=0$, we find for the Hamiltonian in the tilted frame

$$\begin{aligned}\mathcal{H}'_{\rm SRF}(t) &= e^{i\theta S_y}\mathcal{H}_{\rm SRF}(t)e^{-i\theta S_y} \\ &= \omega_{\rm eff}S_z + 2\omega_2\frac{\Omega_S}{\omega_{\rm eff}}\cos(\omega_{\rm rf}t+\varphi_{\rm rf})S_z \\ &\quad - 2\omega_2\frac{\omega_1}{\omega_{\rm eff}}\cos(\omega_{\rm rf}t+\varphi_{\rm rf})S_x,\end{aligned} \tag{9}$$

with $\omega_{\rm eff}=(\Omega_S^2+\omega_1^2)^{1/2}$. A transformation to a toggling frame by a rotation operator analogous to Eq. (4),

$$R'(t) = e^{i[k\omega_{\rm rf}t+(2\omega_2\Omega_S/\omega_{\rm rf}\omega_{\rm eff})\sin(\omega_{\rm rf}t+\varphi_{\rm rf})]S_z}, \tag{10}$$

results in

$$\begin{aligned}\mathcal{H}'_{{\rm TF},k}(t) &= (\omega_{\rm eff}-k\omega_{\rm rf})S_z - \frac{\omega_2\omega_1}{\omega_{\rm eff}}\sum_{n=-\infty}^{+\infty}J_n\left(\frac{2\omega_2\Omega_S}{\omega_{\rm rf}\omega_{\rm eff}}\right) \\ &\quad\times[e^{i[(k+n+1)\omega_{\rm rf}t+(n+1)\varphi_{\rm rf}]S_z}S_x e^{-i[(k+n+1)\omega_{\rm rf}t+(n+1)\varphi_{\rm rf}]S_z} \\ &\quad + e^{i[(k+n-1)\omega_{\rm rf}t+(n-1)\varphi_{\rm rf}]S_z}S_x e^{-i[(k+n-1)\omega_{\rm rf}t+(n-1)\varphi_{\rm rf}]S_z}] \\ &\approx (\omega_{\rm eff}-k\omega_{\rm rf})S_z + \frac{k\omega_1\omega_{\rm rf}}{\Omega_S}J_{-k}\left(\frac{2\omega_2\Omega_S}{\omega_{\rm rf}\omega_{\rm eff}}\right)S_x,\end{aligned} \tag{11}$$

where all higher-order corrections are omitted. Obviously, the term with S_x vanishes for $k=0$. For weak mw fields, $\omega_1 \ll k\omega_{\rm rf}\approx\Omega_S$, the Hamiltonian in Eq. (11) becomes equal to the Hamiltonian in Eq. (8), whereas for $\omega_1 \gg \Omega_S$, we find

$$\begin{aligned}\mathcal{H}'_{{\rm TF},k} &= (\omega_1-k\omega_{\rm rf})S_z + \frac{k\omega_1\omega_{\rm rf}}{\Omega_S}J_{-k}\left(\frac{2\omega_2\Omega_S}{\omega_{\rm rf}\omega_1}\right)S_x \\ &\approx (\omega_1-k\omega_{\rm rf})S_z + \omega_2\frac{k(-1)^k}{|k|!}\left(\frac{\omega_2\Omega_S}{\omega_{\rm rf}\omega_1}\right)^{|k|-1}S_x.\end{aligned} \tag{12}$$

For $|k|>1$, the second term is very small, and zero for $\Omega_S=0$. In practice only the case with $k=1$ is of importance.

The Hamiltonian in Eq. (12) describes *rotary saturation* introduced by Redfield [40]. In this cw NMR experiment in addition to the driving transverse rf field a second field in the audio-frequency range is applied parallel to $\mathbf{B}_0$. When the frequency of this second field equals $\omega_{\rm eff}$, the steady-state transverse magnetization is reduced, which is explained as saturation of the transition induced by the second field in a tilted doubly rotating frame. A similar experiment has recently been carried out in pulse EPR. In pulse dressed EPR, one or several rf pulses applied along the z axis flip the spin coherence that is spin-locked by a high-turning-angle mw pulse [41].

Since for the single-photon transition with $k=0$ the Hamiltonian in Eq. (11) gives only the oversimplified result $\mathcal{H}'_{{\rm TF},0}=\omega_{\rm eff}S_z$, we have to use Eq. (8) for the description of transparency on this transition. For large mw amplitudes, as used in pulse EPR experiments, higher-order effects have to be taken into account.

B. Transparency induced by the longitudinal rf field

We now describe the multiple photon transitions of the type $-m\pi_{\rm rf}+\sigma^+_{\rm mw}+m\pi_{\rm rf}$ in more detail. In the case of a resonant mw field, $\omega_{\rm mw}=\omega_S$ and $k=0$, energy and angular momentum are conserved not only for the single-photon process but also for the $-m\pi_{\rm rf}+\sigma^+_{\rm mw}+m\pi_{\rm rf}$ multiple photon processes [see Fig. 2(a)]. In the single-photon process (1), one mw σ^+ photon is absorbed, whereas in the two three-photon processes (2) with $m=\pm1$ one rf π photon and one mw σ^+ photon are absorbed, and one rf π photon is emitted. Also five-photon processes (3) with $m=\pm2$ and processes of higher order have to be considered. The effective field for the single-photon transition is plotted in Fig. 2(b) as a function of the normalized rf amplitude $z=2\omega_2/\omega_{\rm rf}$, together with the contributions of the processes (1), (1)+(2), and (1)+(2)+(3).

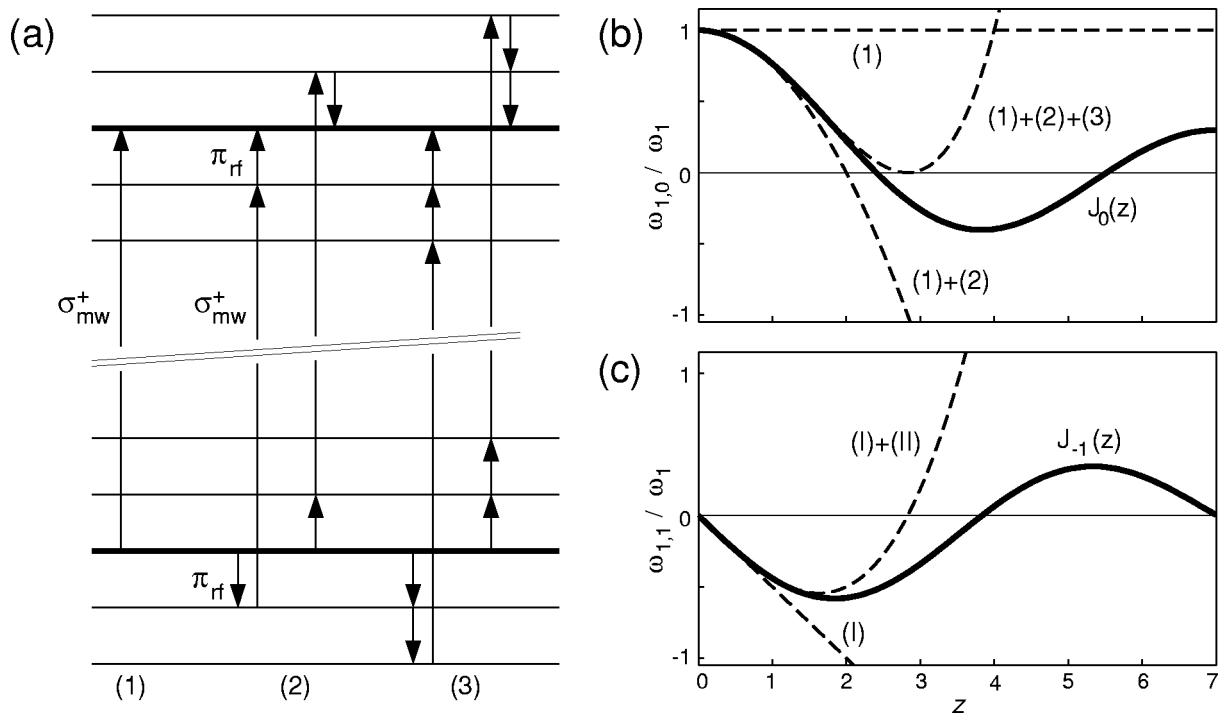

FIG. 2. (a) Multiple photon transitions of the type $-m\pi_{rf}+\sigma^+_{mw}+m\pi_{rf}$, created by a bichromatic radiation field resonant with the single-photon transition, $\omega_{mw}=\omega_S$. (1) Single-photon process σ^+_{mw}; (2) three-photon processes $\pi_{rf}+\sigma^+_{mw}-\pi_{rf}$ and $-\pi_{rf}+\sigma^+_{mw}+\pi_{rf}$; (3) five-photon processes $2\pi_{rf}+\sigma^+_{mw}-2\pi_{rf}$ and $-2\pi_{rf}+\sigma^+_{mw}+2\pi_{rf}$. (b) Effective field $\omega_{1,0}=\omega_1 J_0(z)$ (normalized to the mw field amplitude ω_1) according to Eq. (7) for the center band (σ^+_{mw} transition) at $\omega_{mw}=\omega_S$, as a function of $z=2\omega_2/\omega_{rf}$ (bold solid line). The contributions from the processes (1), (1)+(2), and (1)+(2)+(3) are also given (dashed lines). (c) Effective field $\omega_{1,1}=\omega_1 J_{-1}(z)$ for the first sideband ($\sigma^+_{mw}+\pi_{rf}$ transition) at $\omega_S=\omega_{mw}+\omega_{rf}$ (bold solid line). In analogy to (b) the contributions from the two-photon processes (I) and the four-photon processes (II) are also shown (dashed lines).

For rf amplitudes $z<1$, the effective field can be well approximated by only considering the processes (1) and (2), and for $z<2$ by considering the processes (1), (2), and (3). The effective field amplitude $\omega_{1,0}$ for the absorption of one mw σ^+ photon is given by the sum of the effective field amplitudes of all contributing multiple photon processes,

$$\omega_{1,0}=\omega_1 J_0\left(\frac{2\omega_2}{\omega_{rf}}\right). \tag{13}$$

A corresponding behavior is found for the sidebands, as is shown in Fig. 2(c) for the $\sigma^+_{mw}+\pi_{rf}$ two-photon transition (first sideband, $k=1$), and the corresponding multiple photon processes of the type $-m\pi_{rf}+\sigma^+_{mw}+(m+1)\pi_{rf}$.

There is an alternative to the description in the toggling frame, where the contributions of the different multiple photon processes spanning a certain energy difference are summed up to one effective field amplitude. The dynamics of our two-level spin system could also be treated in terms of a spin system dressed by the (strong) rf field. The weak mw field then induces resonant transitions between such dressed states. A corresponding method was applied by Freedhoff and Chen to calculate the fluorescence spectrum of a two-level atom driven by a strong bichromatic laser field [11]. While the two approaches are equivalent from a physical point of view, the toggling-frame approach is better suited to describe the dynamics of the multiple photon transitions.

Of special interest is the finding that the effective field $\omega_{1,k}$ can be *zero*. The two-level system then becomes transparent. For the center band (single-photon transition) the effective field $\omega_{1,0}$ is zero at the zero crossings of the Bessel function $J_0(z)$. The first zero is at $z=j_{0,1}\approx 2.4048$, the second zero at $z=j_{0,2}\approx 5.5201$, etc. For the two first sidebands [$k=\pm 1$, with $\omega_S=\omega_{mw}\pm\omega_{rf}$, see transitions (1) and (2) in Fig. 1] the effective field $\omega_{1,1}$ is zero at $z=j_{\pm 1,1}\approx 3.8317$, $z=j_{\pm 1,2}\approx 7.0156$, etc.

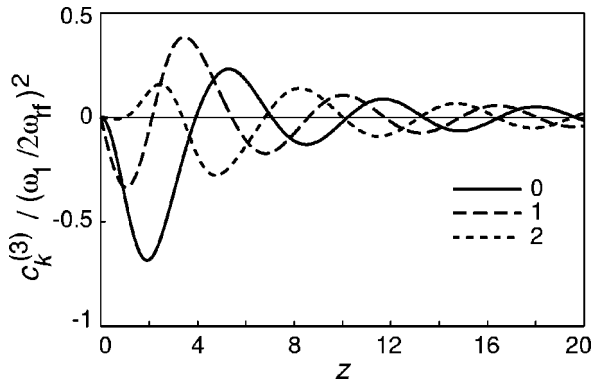

FIG. 3. Third-order contribution $c_k^{(3)}$ to the effective field $\omega_{1,k}$ [see Eq. (7)], normalized to $(\omega_1/2\omega_{rf})^2$, as a function of $z=2\omega_2/\omega_{rf}$, for toggling frames with $k=0,1,$ and 2.

For larger mw amplitudes the third-order contribution $c_k^{(3)}$ in Eq. (7) causes a shift of the zero crossings. Figure 3 shows plots of $c_k^{(3)}$ as a function of z, for toggling frames with $k=0,1$, and 2. For the center band, $|c_0^{(3)}|$ is maximum close to the first zero crossing. The zero crossing of the effective field amplitude $\omega_{1,0}$ is shifted to smaller values of z, as is shown for a selection of values $\omega_1/\omega_{\mathrm{rf}}$:

$\omega_1/\omega_{\mathrm{rf}}$	$j_{0,1}^{\mathrm{corr}}$
0	2.4048
0.25	2.3866
0.50	2.3306
0.75	2.2345

C. Phase of the effective field

A bichromatic pulse, resonant with a $\sigma_{\mathrm{mw}}^{+}+k\pi_{\mathrm{rf}}$ multiple photon transition, excites also other $\sigma_{\mathrm{mw}}^{+}+l\pi_{\mathrm{rf}}$ multiple photon transitions, with $l\neq k$. The signals caused by these transitions can be partially removed by appropriate rf phase cycles. The phases

$$\varphi_k=\varphi_{\mathrm{mw}}+k\varphi_{\mathrm{rf}} \tag{14}$$

of the effective fields $\omega_{1,k}$ in the corresponding toggling frames show different dependences on the rf phase. In Table I we have evaluated Eq. (14) for a number of values of the rf phase φ_{rf}, in different toggling frames with $k=-3,\ldots,3$. The mw phase was set to $x(\varphi_{\mathrm{mw}}=0)$. A change of the rf phase by π, for example, has different effects on the effective fields. While for the toggling frame describing the single-photon transition the phase φ_0 does not change, the effective fields of the two-photon transitions experience a change in phase by π, resulting in $\varphi_{\pm1}=-x$.

When the rf phase cycle $[(0)-(\pi)]$ is applied, the signals generated by the single-photon and the $\sigma_{\mathrm{mw}}^{+}\pm2\pi_{\mathrm{rf}}$ three-photon transitions (and all other transitions with an even number of rf photons) are eliminated, but not the signals of the $\sigma_{\mathrm{mw}}^{+}\pm\pi_{\mathrm{rf}}$ transitions and all other transitions with an odd number of rf photons. The rf phase cycle $[(0)-(\pi/2)+(\pi)-(3\pi/2)]$, on the other hand, selects the three-photon transitions and removes the signals of the one- and two-photon transitions. This procedure can be extended to a random rf phase. Averaging over a sufficiently large number of experiments then leads to a complete removal of all coherences on the sidebands, and only coherence on the single-photon transition remains.

TABLE I. Phase $\varphi_k=\varphi_{\mathrm{mw}}+k\varphi_{\mathrm{rf}}$ of the effective field $\omega_{1,k}$ in the kth toggling frame, for a mw phase $x(\varphi_{\mathrm{mw}}=0)$ and rf phases $\varphi_{\mathrm{rf}}=0$, $\pi/2$, π, and $3\pi/2$.

φ_{rf}		0	$\frac{1}{2}\pi$	π	$\frac{3}{2}\pi$
	3	x	$-y$	$-x$	y
	2	x	$-x$	x	$-x$
	1	x	y	$-x$	$-y$
k	0	x	x	x	x
	−1	x	$-y$	$-x$	y
	−2	x	$-x$	x	$-x$
	−3	x	y	$-x$	$-y$

When the density operator is transformed to a toggling frame, polarization remains unaffected, while coherence that is already present experiences a phase shift

$$\Delta\varphi=-k\omega_{\mathrm{rf}}t-\left(\frac{2\omega_2}{\omega_{\mathrm{rf}}}\right)\sin(\omega_{\mathrm{rf}}t+\varphi_{\mathrm{rf}}), \tag{15}$$

caused by the rotation operator in Eq. (4). Since the phase shift of the coherence [Eq. (15)] and the phase shift of the effective field [Eq. (14)] are different, rf phase cycles are preferably applied when no coherence is present.

III. VECTOR MODEL

One might be tempted to describe the investigated transparency phenomenon, by using an oversimplified qualitative approach, in which the longitudinal rf field is treated as constant over short-time intervals. From such a point of view the transparency would just be the result of a reduced amount of time during which the spin system is resonant with the mw field. An increase in rf amplitude thus would lead to a decrease of the averaged absorbed mw power. This simple view, however, clearly contradicts the findings presented in Sec. II and fails to predict the distinct rf field amplitudes for which transparency occurs.

In the following we give a classical description of the transparency effects based on the equation of motion for the magnetization vector **M**. Two borderline cases are discussed.

(1) Starting from thermal equilibrium. The magnetization vector is oriented along $\mathbf{B}_0$, and only spin polarization exists.

(2) Starting from transverse magnetization. Only spin coherence exists.

For both cases numerically calculated trajectories that describe the motion of the tip of **M** are shown for weak and strong mw amplitudes. In addition, we also discuss the effects caused by inhomogeneous lines. In all the simulations a radio frequency of $\omega_{\mathrm{rf}}/2\pi=10$ MHz is used.

A. Polarization

First we consider the behavior of **M** under a bichromatic pulse starting from longitudinal magnetization.

1. Weak mw field

For a weak mw field with amplitude $\omega_1/2\pi=0.01$ MHz, as it is typically used in cw EPR experiments, the third-order term $c_k^{(3)}$ in Eq. (7) is negligible. The first transparency condition for the single-photon transition is thus reached at $z=j_{0,1}=2.4048$. Starting from thermal equilibrium a bichromatic pulse is applied, with a mw field ω_1 along the x axis of the rotating frame and a rf field $2\omega_2\sin(\omega_{\mathrm{rf}}t)$ along the z axis. The magnetization vector **M** describes a figure of eight, very close to the z axis [Fig. 4(a)]. The motion of **M** can be described as follows: For $t=0$ the effective field vector is given by $\boldsymbol{\omega}_{\mathrm{eff}}=\boldsymbol{\omega}_1$, and **M** nutates around the x axis. Since

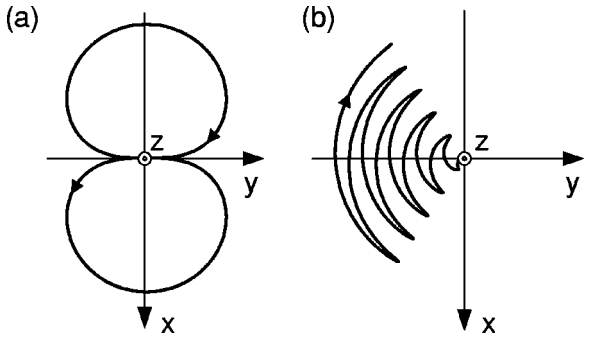

FIG. 4. Motions of the magnetization vector **M** under a bichromatic field, starting from thermal equilibrium (**M** along the *z* axis). The weak mw field, $\omega_1/2\pi=0.01$ MHz, is resonant with the single-photon transition. Projections onto the *xy* plane. (a) Transparency condition fulfilled, $z=2.4048$. The magnetization vector describes a figure of eight close to the *z* axis, reaching a maximum deviation angle from the *z* axis of 0.07°. (b) Transparency condition not fulfilled, $z=1$. The magnetization vector moves to the *xy* plane. The trajectory is shown for the first five rf periods. The scaling of the axes is reduced by the factor 20, compared to (a).

$\omega_2 \gg \omega_1$, the angle between the effective field $\boldsymbol{\omega}_{\text{eff}}$ and the *z* axis gets rapidly very small, and the magnetization nutates virtually around the *z* axis. After one quarter of a rf period we have $\boldsymbol{\omega}_{\text{eff}} \approx 2\boldsymbol{\omega}_2$. The magnetization is in the *xz* plane, and has reached its maximum deviation from the *z* axis (0.07°). At $t=\pi/\omega_{\text{rf}}$ (half of a rf period) the effective field is again $\boldsymbol{\omega}_{\text{eff}}=\boldsymbol{\omega}_1$, and at the same time **M** is oriented exactly along the *z* axis. During the next half of a rf period the effective field is $\boldsymbol{\omega}_{\text{eff}} \approx -2\boldsymbol{\omega}_2$. Correspondingly, **M** describes a symmetric trajectory with corresponding negative *x* values. After a full rf period, **M** is again oriented along the *z* axis, and the figure of eight is closed.

If the transparency condition is not fulfilled, the trajectory is no longer a closed curve, and the magnetization moves on a toggling path towards the *xy* plane, as shown in Fig. 4(b) for $z=1$ and the first five rf periods. In the toggling frame with $k=0$, the movement would appear as a nutation to the *xy* plane around the effective field vector $\boldsymbol{\omega}_{1,0}$.

2. Strong mw field

For strong mw fields, as they are used in pulse EPR experiments, higher-order contributions to the effective field become relevant. This reduces the value of *z* for which transparency is observed. For a mw amplitude $\omega_1/2\pi=5$ MHz, corresponding to a π pulse of length 100 ns, transparency occurs at $z=2.3306$ instead of $z=2.4048$.

For the resonant case the tip of **M** describes again a figure of eight, but with larger maximum deviation from the *z* axis [see Fig. 5(a)]. When the mw field is off-resonant, the trajectory is distributed over a wider area on the unit sphere. This is shown in Fig. 5(b) for a resonance offset of $\Omega_S/2\pi=5$ MHz. Although for both the on-resonant and off-resonant case the spin system is still transparent for the single-photon transition, the multiple photon transitions have nonzero transition amplitudes. This is the reason for the larger deviation of **M** from the *z* axis.

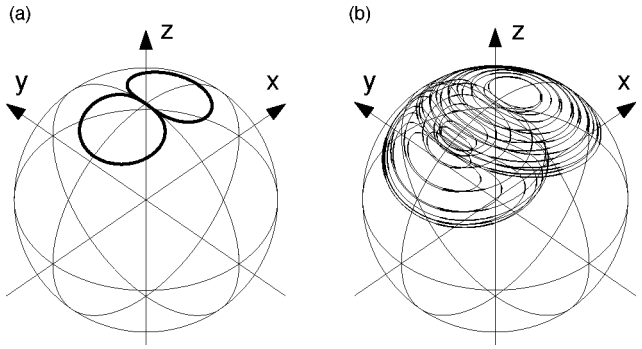

FIG. 5. Motions of the magnetization vector **M** under a bichromatic field, starting from thermal equilibrium (**M** along the *z* axis). Strong mw field, $\omega_1/2\pi=5$ MHz. (a) On-resonant mw field, the transparency condition $z=2.3306$ is fulfilled. The magnetization vector describes a figure of eight. (b) Off-resonant mw field, $\Omega_S/2\pi=5$ MHz.

B. Coherence

We now consider the behavior **M** under a bichromatic field starting from transverse magnetization along the $-y$ axis.

1. Weak mw field

With the same parameters as in Sec. III A 1 the magnetization along the $-y$ axis essentially experiences only the rf field ($\omega_2 \gg \omega_1$). Since for the first half of a rf period the off-resonance caused by the rf field is positive, the magnetization moves in the right-hand sense close to the *xy* plane, with a small negative *z* component due to the weak mw field. After half of a rf period, **M** is again in the *xy* plane, and has accumulated a phase of about 280° with respect to the starting position. During the second half of the rf period, **M** experiences the same off-resonance field but with opposite sign, and thus moves back with a small positive *z* component. After one full rf period **M** reaches again the $-y$ axis. The resulting trajectory is shown in Fig. 6(a).

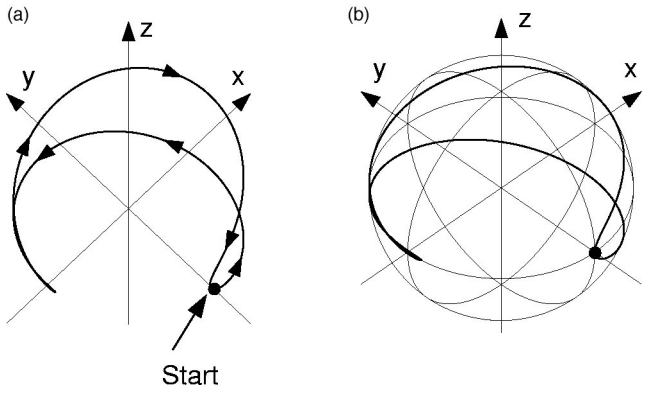

FIG. 6. Motions of the magnetization vector **M** under a resonant bichromatic field, $\omega_{\text{mw}}=\omega_S$, starting from transverse magnetization along the $-y$ axis. (a) Weak mw field, $\omega_1/2\pi=0.01$ MHz, $z=(2\omega_2/\omega_{\text{rf}})=2.4048$. The *z* axis is stretched by a factor 1000 for better visibility. (b) Strong mw field, $\omega_1/2\pi=5$ MHz, $z=2.3306$.

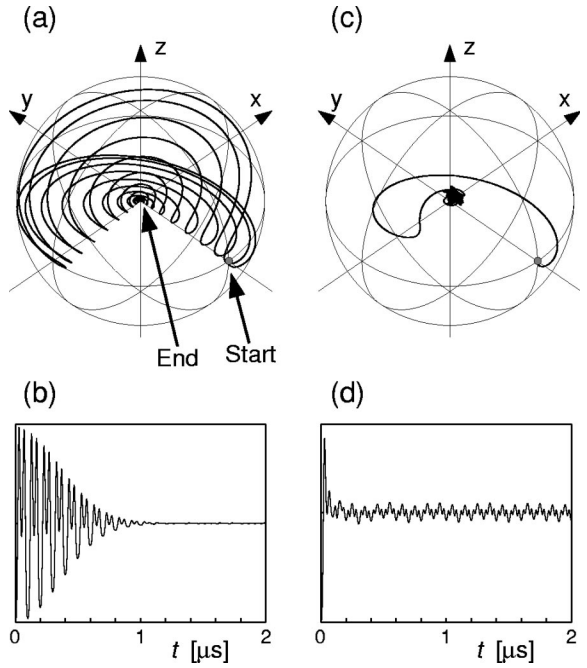

FIG. 7. Motions of the magnetization vector **M** for inhomogeneously broadened lines under a bichromatic field, $\omega_1/2\pi = 5$ MHz, $z = 2.3306$, starting from transverse magnetization along the $-y$ axis. (a) Linewidth $\Gamma_{\mathrm{FWHH}} = 1$ MHz. (b) Corresponding FID detected along the y axis. (c) Linewidth $\Gamma_{\mathrm{FWHH}} = 10$ MHz. The line partially overlaps with the two-photon transitions $\sigma^+ \pm \pi$ at $\omega_S \pm \omega_{\mathrm{rf}}$. (d) Corresponding FID detected along the y axis. The residual signal for $t > 0.2$ μs is due to the two-photon transitions that are resonant with part of the line.

2. Strong mw field, inhomogeneous lines

For the great majority of paramagnetic systems the lines are inhomogeneously broadened. It is therefore of interest to investigate the behavior of such spin systems under a bichromatic pulse. For strong mw fields the maximum z component of **M** during transparency gets larger than for the case of a weak mw field [see Fig. 6(b)]. Figure 7(a) shows the dephasing of the magnetization after application of a nonselective $\pi/2$ pulse to a spin system with an inhomogeneous line of width $\Gamma_{\mathrm{FWHH}} = 1$ MHz (FWHH: full width at half height). Due to the applied rf field, the observed free induction decay (FID), shown in Fig. 7(b), manifests as a damped oscillation instead of a monotonic decay. The corresponding situation for an inhomogeneous line of width $\Gamma_{\mathrm{FWHH}} = 10$ MHz is shown in Fig. 7(c). The residual transverse magnetization observed after the rapidly decaying FID [Fig. 7(d)] is mainly caused by the two-photon transitions $\sigma^+_{\mathrm{mw}} \pm \pi_{\mathrm{rf}}$, since their resonance positions lie now within the linewidth. The effective field of these transitions is not zero, causing an oscillatory steady-state signal.

IV. EXPERIMENT

The bichromatic pulse experiments were carried out on a Bruker Elexsys E580 X-band spectrometer. The rf field parallel to the static magnetic field was produced by the rf coil of a pulse ENDOR probehead (Bruker ER 4118X-MD5-EN) rotated by 90°. The rf was amplified by a broadband amplifier (Amplifier Research, model 250A250A).

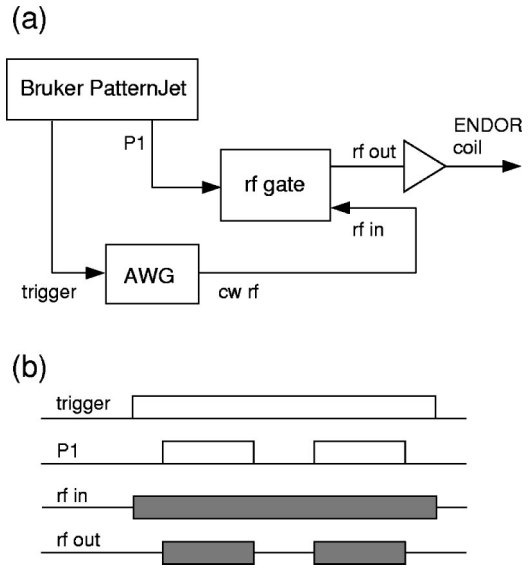

FIG. 8. (a) Block diagram of the setup used for the rf phase cycling of bichromatic pulses. (b) Corresponding triggers and rf pulses.

The setup for the generation of bichromatic pulses and the pulse and trigger times are shown in Fig. 8. A stable rf phase, fixed with respect to the pulse sequence, was obtained by feeding a long pulse trigger, which covers the complete pulse sequence, to an arbitrary wave-function generator (LeCroy LW420B). The rf pulses applied during the mw pulses were then generated from this reference rf pulse by a rf gate, using the two rf pulse triggers ("P1" and "P2") of the PatternJet pulse programmer unit of the Elexsys console.

The relative amplitude of the rf field was measured via the output peak-to-peak voltage of the ENDOR coil. The conversion factor between this voltage and the rf amplitude was determined by a Davies-ENDOR nutation experiment on protons. This allowed us to check the plausibility of the proposed dependence of the effective field on the parameter $z = 2\omega_2/\omega_{\mathrm{rf}}$, with an accuracy of about 20%. The error is caused by the different characteristics of the experimental setup for the proton-ENDOR frequency of about 14 MHz and the 10 MHz rf field used in Secs. V A and V B.

V. EXPERIMENTAL VERIFICATIONS

To verify the predicted dependency of the effective field on the rf amplitude and to show the feasibility of the transparency induced by the longitudinal field, two types of experiments were carried out. Delocalized radicals in coal were used as a two-level model system. All experiments were done at room temperature.

A. Nutation experiment

In this experiment the nutation of the magnetization vector (starting from thermal equilibrium) during a bichromatic

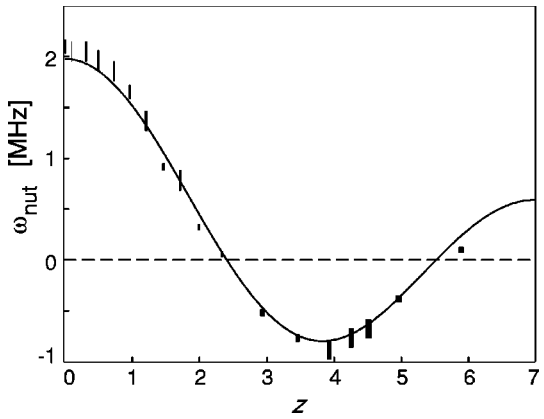

FIG. 9. FID-detected nutation experiment on coal (ω_{mw}: X-band, room temperature, $\omega_{rf}/2\pi=10$ MHz). The nutation frequency during a bichromatic pulse, resonant with the single-photon transition, is plotted as a function of $z=2\omega_2/\omega_{rf}$ (rectangles show the error limits). Full line: theoretical expression $\omega_1 J_0(z)$ fitted to the experimental data.

pulse, with the mw frequency resonant with the center of the line, is recorded as a function of the rf parameter $z=(2\omega_2/\omega_{rf})$ by integrating over the FID that follows the pulse. For a radio frequency $\omega_{rf}/2\pi=10$ MHz and a fixed rf amplitude ω_2 the pulse length is incremented from 0 to 8 μs, in steps of 10 ns. According to Eq. (15), the phase of the observed signal is shifted by $\Delta\varphi(t_p)=(2\omega_2/\omega_{rf})\sin(\omega_{rf}t_p)$. Although the resulting additional oscillation of the signal has a large amplitude, it does not interfere with the nutation and has thus no influence on the results. After Fourier transformation of the time trace the nutation frequency is obtained, which gives the effective field amplitude $\omega_{1,0}$ of the single-photon transition.

The results are plotted in Fig. 9 as a function of $z=2\omega_2/\omega_{rf}$. The nutation frequency is maximum for $z=0$, and decreases with increasing z. For $z\approx 2.4$ the nutation frequency is zero, and the magnetization vector essentially remains oriented along the z axis; the spin system is transparent. For $2.4<z<5.5$ the nutation frequency increases again, with a phase change of 180° due to the negative sign of $\omega_{1,0}$. For $z\approx 5.52$ [second zero crossing of $J_0(z)$] the spin system is again transparent to the mw radiation. The theoretically predicted nutation frequency $\omega_{1,0}=\omega_1 J_0(z)$ is in good agreement with the experimental data. The third-order contribution $c_k^{(3)}$ to the effective field defined in Eq. (7) is negligible, since for the used radio frequency $\omega_{rf}/2\pi=10$ MHz and mw amplitude $\omega_1/2\pi\approx 2.1$ MHz (estimated from the nutation frequency caused by the mw pulse alone), $c_0^{(3)}$ shifts the zero crossing by less than 1 %.

B. Two-pulse echo experiment

In the second experiment the intensity of a primary echo, created by a two-pulse sequence consisting of a bichromatic pulse and a monochromatic mw pulse, is measured as a function of the rf parameter $z=(2\omega_2/\omega_{rf})$. The pulse sequence is shown in Fig. 10(a). The effective flip angle of the first

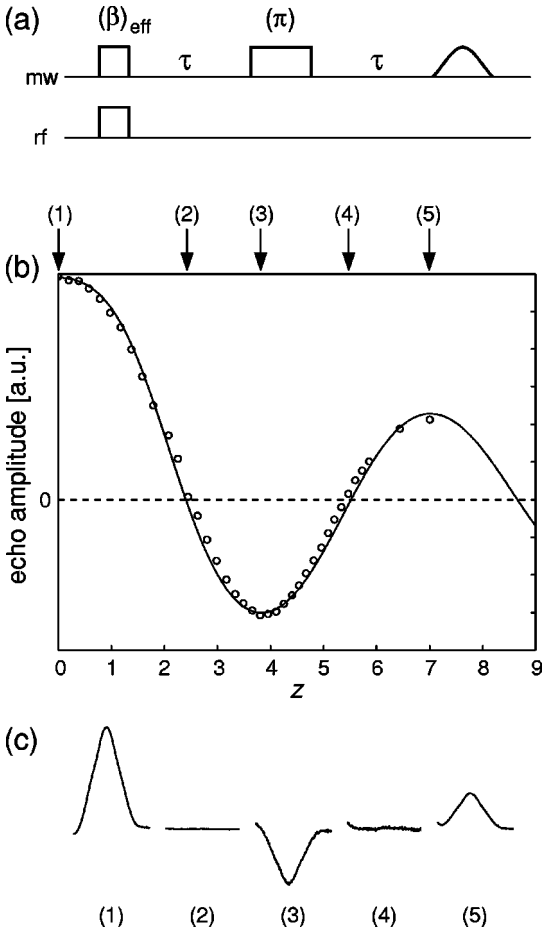

FIG. 10. Two-pulse echo experiment $(\beta)_{eff}-\tau-(\pi)_{mw}-\tau-(echo)$ on coal (ω_{mw}: X-band, room temperature, $\omega_{rf}/2\pi=10$ MHz). (a) Pulse sequence, length of the bichromatic pulse— 200 ns, length of the monochromatic π pulse— 400 ns, $\tau=600$ ns. (b) Integrated echo amplitude as a function of $z=2\omega_2/\omega_{rf}$. Circles: experimental data. Full line: fitted theoretical echo amplitude $\propto\sin[\beta_1 J_0(z)]$. (c) Echoes observed for z values marked by arrows (1)–(5) in plot (b).

(bichromatic) pulse is proportional to the effective field in the toggling frame of the single-photon transition,

$$\beta_{eff}=\omega_{1,0}t_p=\omega_1 J_0(z)t_p. \tag{16}$$

In a standard two-pulse echo experiment the echo intensity is proportional to $\sin(\beta_1)\sin^2(\beta_2/2)$, with the flip angles β_1 and β_2 of the first and second pulse [38]. For the echo intensity I observed with the sequence in Fig. 10(a) we thus expect

$$I\propto\sin[\beta_1 J_0(z)], \tag{17}$$

with the nominal maximum flip angle $\beta_1=\omega_1 t_p$. The experimentally observed echo intensities as a function of the rf parameter z are shown in Fig. 10(b). The pulse lengths were 200 ns for the bichromatic pulse and 400 ns for the monochromatic pulse. The delay time was $\tau=600$ ns, and the flip angle β_1 of the first pulse was slightly smaller than $\pi/2$. The radio frequency $\omega_{rf}/2\pi=10$ MHz was kept con-

stant and the rf amplitude ω_2 was varied. The experimental data were fitted with good agreement by Eq. (17).

The echoes observed at five particular rf fields are shown in Fig. 10(c). Without rf field ($z=0$, position 1) the echo signal is maximum. With increasing z the flip angle β_{eff} and thus also the echo decrease. For $z\approx 2.4$ the spin system is transparent to the first pulse, so that no coherence is created that could be refocused to an echo by the second pulse (position 2). For $2.4<z<5.5$ the echo changes its phase and reaches the maximum amplitude at $z\approx 3.9$ (position 3). The second zero crossing is found for $z\approx 5.5$ (position 4) and the next local maximum is reached at $z\approx 7.2$ (position 5).

VI. ONE-PULSE ECHO

Bichromatic pulses can be used as a tool to control experimentally the transition amplitude, including the full suppression of the interaction of the mw field with the spin system. As an example we demonstrate that an electron-spin echo can be generated with a *single* mw pulse, when during part of this pulse a free evolution period is artificially created by a rf pulse, with a field amplitude that fulfills the first transparency condition.

In such a one-pulse echo experiment with a mw pulse of length t_{mw}, a rf pulse of length τ_1 is turned on at time t_{p1} and turned off at time $t_{\text{mw}}-t_{\text{p2}}$, with $2t_{\text{p1}}=t_{\text{p2}}$ and $\tau_1=t_{\text{mw}}-t_{\text{p1}}-t_{\text{p2}}$ [see Fig. 11(a)]. Nominal flip angles $\beta_1=\pi/2$ during t_{p1} and $\beta_2=\pi$ during t_{p2} are used. The pulse scheme thus corresponds to a two-pulse echo sequence, $(\pi/2)-\tau_1-(\pi)-\tau_2-(\text{echo})$, with an artificial free evolution period of time τ_1, and a normal free evolution period of length $\tau_2=\tau_1$. During time τ_1 the spin coherence evolves as it would do during a free evolution period, except from a phase shift depending on $z=2\omega_2/\omega_{\text{rf}}$, the rf phase, and the length of the bichromatic pulse [see Eq. (15)].

Figure 11(b) shows experimental time traces for mw pulse lengths $t_{\text{mw}}=1.3-3.1\ \mu$s and rf pulse lengths $\tau_1=0.4-2.2\ \mu$s, and fixed times $t_{\text{p1}}=300$ ns and $t_{\text{p2}}=600$ ns. The radio frequency was 15 MHz. The signal that follows the mw pulse consists of a FID and an echo at time $\tau_2=\tau_1$, as in a conventional two-pulse echo sequence. The rf phase was optimized for maximum echo amplitude. Since τ_1 was increased in steps that were multiples of the rf period, the phase shift according to Eq. (15) was zero.

This experiment successfully demonstrates that an artificial free evolution period can be created during a mw pulse, in which the spin coherence is not destroyed by the mw field.

VII. CONCLUSIONS

We have shown theoretically and experimentally that a two-level spin system can become transparent to mw radiation under the influence of a longitudinal rf field. The experimental results demonstrate that the theory based on the toggling-frame approach correctly describes the behavior of a spin system excited by bichromatic pulses. For certain values of the rf field amplitude the electron-spin system becomes transparent to the mw field. To illustrate the behavior of the spin system under the combined mw and rf radiation,

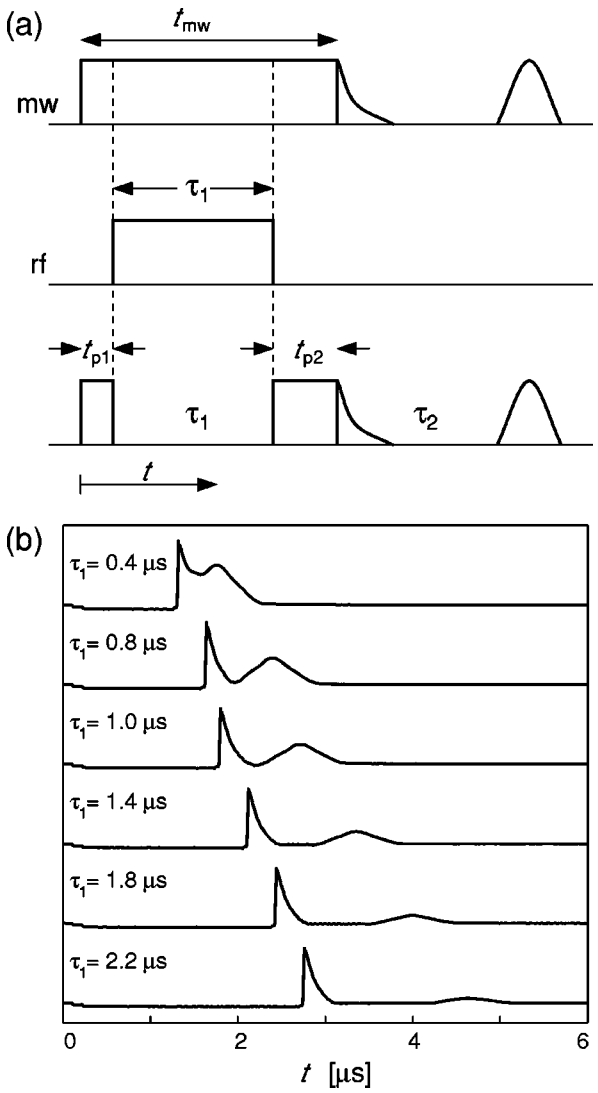

FIG. 11. One-pulse echo experiment with an artificial free evolution period on a coal sample at room temperature, $\omega_{\text{mw}}/2\pi=9.626$ GHz (X-band), $\omega_{\text{rf}}/2\pi=15$ MHz, and $B_0=341.1$ mT. (a) The pulse sequence shows the mw, rf, and resulting effective fields acting on the single-photon transition of the spin system. $t_{\text{p1}}=300$ ns, $t_{\text{p2}}=600$ ns, $t_{\text{mw}}=1.3-3.1\ \mu$s, and $\tau_1=0.4-2.2\ \mu$s. During the time interval τ_1 a rf pulse is applied, with the normalized rf field amplitude $z=2\omega_2/\omega_{\text{rf}}$ which fulfills the first transparency condition for the single-photon transition. (b) Experimental time traces showing FIDs and echoes for different τ_1 values.

we showed examples of numerically calculated trajectories described by the tip of the magnetization vector. Finally, the phenomenon of an artificially induced free evolution during a bichromatic pulse is verified by a one-pulse echo experiment.

There are several potential applications of the observed transparency effect in EPR spectroscopy. In a number of pulse EPR techniques two mw fields with frequencies $\omega_{\text{mw},1}$ and $\omega_{\text{mw},2}=\omega_{\text{mw},1}+\Delta\omega$ are used to excite different spin packages. The mw field $\omega_{\text{mw},2}$ can then be replaced by a bichromatic field with frequencies $\omega_{\text{mw},1}$ and $\omega_{\text{rf}}=|\Delta\omega|$. If the rf field fulfills the transparency condition for the single-photon transition, a bichromatic pulse with this rf field will excite

spin packages resonant for $\omega_S = \omega_{mw,1} \pm \omega_{rf}$, but not the ones resonant for $\omega_S = \omega_{mw,1}$. The effective field amplitude for the transitions with $\omega_S = \omega_{mw}$ is zero.

Bichromatic pulses have already been successfully implemented in two-pulse EPR experiments [42], namely, in *stimulated soft electron-spin-echo envelope modulation* (ESEEM), allowing the observation of nuclear frequencies with selective mw pulses [43], and in *double electron-electron resonance* for the determination of distances between electron spins [44]. Other potential candidates for bichromatic pulses are pulse ELDOR-detected NMR, an alternative to ESEEM in cases when the forbidden transitions are very weak [45], and hyperfine-selective ENDOR, a two-dimensional method in which the ENDOR spectrum is disentangled into a second dimension, representing the hyperfine couplings [46,47].

The influence of relaxation on the robustness of the transparency effect, which is of major importance in optical transparency experiments, has not been addressed in this work. Owing to the very low frequencies used in EPR spectroscopy, compared to experiments in the optical regime, spontaneous emission is negligible. Relaxation, however, is present in the form of transverse relaxation of coherence and longitudinal relaxation of polarization. The studied bichromatic field experiments showed qualitatively a similar behavior as in standard pulse EPR experiments. The investigated transparency effect was also successfully observed in different paramagnetic systems such as transition-metal complexes (crystals, glasses, powders), radicals, and biradicals. We therefore think that relaxation is of minor importance for the quality of the transparency effect. Nevertheless it would be of interest if there are, for example, modified relaxation mechanisms for coherences and polarizations between different dressed states.

Finally, it should be mentioned that the multiple photon processes discussed in this work, including transparency induced by a longitudinal field, are not restricted to electron spins. Similar effects principally could also be achieved with nuclear spins, allowing the implementation of novel experimental approaches in NMR spectroscopy.

ACKNOWLEDGMENTS

The authors wish to thank Jörg Forrer for technical assistance. This research was supported by the Swiss National Science Foundation.

[1] S. L. McCall and E. L. Hahn, Phys. Rev. **183**, 457 (1969).
[2] S. B. Grossman and E. L. Hahn, Phys. Rev. A **14**, 2206 (1976).
[3] K.-J. Boller, A. Imamoğlu, and S. E. Harris, Phys. Rev. Lett. **66**, 2593 (1991).
[4] D. J. Fulton, S. Shepherd, R. R. Moseley, B. D. Sinclair, and M. H. Dunn, Phys. Rev. A **52**, 2302 (1995).
[5] S. E. Harris, Phys. Today **50**(7), 36 (1997).
[6] G. S. Agarwal, Phys. Rev. A **55**, 2467 (1997).
[7] R. Rakhmatullin, E. Hoffmann, G. Jeschke, and A. Schweiger, Phys. Rev. A **57**, 3775 (1998).
[8] C. Wei and N. B. Manson, Phys. Rev. A **60**, 2540 (1999).
[9] C. Wei and N. B. Manson, J. Opt. B: Quantum Semiclassical Opt. **1**, 464 (1999).
[10] R. S. Bennink, R. W. Boyd, C. R. Stroud, and V. Wong, Phys. Rev. A **63**, 033804 (2001).
[11] H. Freedhoff and Z. Chen, Phys. Rev. A **41**, 6013 (1990).
[12] H. Freedhoff and Z. Chen, Phys. Rev. A **46**, 7328 (1992).
[13] S. P. Tewari and M. K. Kumari, Phys. Rev. A **41**, 5273 (1990).
[14] G. S. Agarwal, Y. Zhu, D. J. Gauthier, and T. W. Mossberg, J. Opt. Soc. Am. B **8**, 1163 (1991).
[15] D. L. Aronstein, R. S. Bennink, R. W. Boyd, and C. R. Stroud, Phys. Rev. A **65**, 067401 (2002).
[16] Z. Ficek, in *Progress in Optics*, edited by E. Wolf (Elsevier, Amsterdam, 2000), Vol. 40, p. 389.
[17] Z. Ficek and H. S. Freedhoff, Phys. Rev. A **48**, 3092 (1993).
[18] Y. Zhu, Q. Wu, A. Lezama, D. J. Gauthier, and T. W. Mossberg, Phys. Rev. A **41**, 6574 (1990).
[19] J. S. Hyde, P. B. Sczaniecki, and W. Froncisz, J. Chem. Soc., Faraday Trans. 1 **85**, 3901 (1989).
[20] P. B. Sczaniecki and J. S. Hyde, J. Chem. Phys. **94**, 5907 (1991).
[21] H. S. Mchaourab and J. S. Hyde, J. Chem. Phys. **98**, 1786 (1993).
[22] P. Bucci, P. Cavaliere, and S. Santucci, J. Chem. Phys. **52**, 4041 (1970).
[23] P. Bucci, M. Martinelli, and S. Santucci, J. Chem. Phys. **53**, 4524 (1970).
[24] Y. Zur, M. H. Levitt, and S. Vega, J. Chem. Phys. **78**, 5293 (1983).
[25] E. M. Krauss and S. Vega, Phys. Rev. A **34**, 333 (1986).
[26] G. Goelman, D. B. Zax, and S. Vega, J. Chem. Phys. **87**, 31 (1987).
[27] J. Burget, M. Odehnal, V. Petříček, J. Šàcha, and L. Trlifaj, Czech. J. Phys. B **11**, 719 (1961).
[28] I. Gromov and A. Schweiger, J. Magn. Reson. **146**, 110 (2000).
[29] M. Kälin, I. Gromov, and A. Schweiger, J. Magn. Reson. **160**, 166 (2003).
[30] M. Kälin, Ph.D thesis, ETH Zürich, 2003 (unpublished), http://e-collection.ethbib.ethz.ch/cgi-bin/show.pl?type=diss&nr=15142
[31] R. Boscaino, F. M. Gelardi, and G. Messina, Phys. Rev. A **28**, 495 (1983).
[32] R. Boscaino, I. Ciccarello, C. Cusumano, and M. W. P. Strandberg, Phys. Rev. B **3**, 2675 (1971).
[33] R. Boscaino, F. M. Gelardi, and G. Messina, Solid State Commun. **46**, 747 (1983).
[34] R. Boscaino, F. M. Gelardi, and G. Messina, Phys. Lett. **97A**, 413 (1983).
[35] B. Clerjaud and A. Gelineau, Phys. Rev. Lett. **48**, 40 (1982).
[36] C. A. Michal, J. Chem. Phys. **118**, 3451 (2003).
[37] P. Lehtovuori and H. Joela, J. Phys. Chem. A **106**, 3061 (2002).

[38] A. Schweiger and G. Jeschke, *Principles of Pulse Electron Paramagnetic Resonance* (Oxford University Press, Oxford, 2001).
[39] F. Bloch and A. Siegert, Phys. Rev. **57**, 522 (1940).
[40] A. G. Redfield, Phys. Rev. **98**, 1787 (1955).
[41] G. Jeschke, Chem. Phys. Lett. **301**, 524 (1999).
[42] M. Fedin, M. Kälin, I. Gromov, and A. Schweiger, J. Chem. Phys. **120**, 1361 (2004).
[43] E. J. Hustedt, A. Schweiger, and R. R. Ernst, J. Chem. Phys. **96**, 4954 (1992).
[44] M. Pannier, S. Veit, A. Godt, G. Jeschke, and H. W. Spiess, J. Magn. Reson. **142**, 331 (2000).
[45] P. Schosseler, T. Wacker, and A. Schweiger, Chem. Phys. Lett. **224**, 319 (1994).
[46] C. Bühlmann, A. Schweiger, and R. R. Ernst, Chem. Phys. Lett. **154**, 285 (1989).
[47] H. Thomann and M. Bernardo, Chem. Phys. Lett. **169**, 5 (1990).